JOURNAL OF MATERIALS SCIENCE 18 (1983) 3117–3127

Electrical conductivity of Sc_2O_3–ZrO_2 compositions by 4-probe d.c. and 2-probe complex impedance techniques

S. P. S. BADWAL
CSIRO Division of Materials Science, Advanced Materials Laboratory, PO Box 4331, Melbourne, Victoria, Australia 3001

The ionic conductivities of several samples in the Sc_2O_3–ZrO_2 system (Sc_2O_3: ~ 8 mol %) have been measured using 4-probe d.c. and 2-probe complex impedance dispersion techniques. Samples which contained monoclinic zirconia showed hysteresis effects and S-shaped Arrhenius conductivity plots. This behaviour was assigned to the m-ZrO_2 ⇌ t-ZrO_2 transformation. In samples which were free of monoclinic ZrO_2, contributions from the grain boundary resistance were relatively small. The Arrhenius plots of their conductivity showed a distinct change in the slope around 600° C towards higher activation energy and this was attributed to vacancy trapping. The 4-probe d.c. data could be fitted to an equation of the form $\rho = A_1T \exp(E_1/RT) + A_2T \exp(E_2/RT)$. The process which dominated the conduction mechanism at lower temperatures had an activation energy of 130 to 140 kJ mol^{-1}. The activation energy for the migration of oxygen ion vacancies within the bulk of the grain was 64 to 70 kJ mol^{-1}.

1. Introduction

Zirconia-based electrolytes are commonly used in high temperature fuel cells, steam electrolysis and for potentiometric gas analysis [1–3]. Zirconia exists in three structural modifications. Monoclinic zirconia (m-ZrO_2) is stable up to ~ 1170° C. Above this temperature it transforms to a tetragonal structure (t-ZrO_2) with ~ 4% reduction in volume [4]. The reverse transformation takes place between 850 and 1000° C during cooling. The highest temperature modification (above 2370° C) has a fluorite structure and is not stable at lower temperatures. However, with the addition of dopants such as CaO, MgO, Y_2O_3, Sc_2O_3 and rare earth oxides the fluorite lattice can be completely or partially stabilized down to room temperature. The aliovalent ions also create anion vacancies in the crystal structure resulting in increased oxygen ion conductivity. The magnitude of this ionic conductivity is a significant criterion in determining the low temperature limit of ZrO_2-based solid state electrochemical devices. It is influenced by dopant concentration, grain size, vacancy trapping by aliovalent cations, ordering of vacancies and above all by second phases at the grain boundaries. With the development of the complex impedance dispersion technique, it is possible to separate contributions due to bulk resistance of the grains and grain boundary resistance [5].

Sc_2O_3–ZrO_2 fluorite-related solid solutions have been reported to have a higher conductivity than other ZrO_2 based electrolytes [6]. The maximum value of conductivity in the Sc_2O_3–ZrO_2 system was reported for Sc_2O_3 concentrations close to 8 mol % [7, 8].

The phase diagram for the Sc_2O_3–ZrO_2 system near the ZrO_2 rich region is complex and has not yet been fully resolved [9, 10]. The 8 mol % Sc_2O_3–ZrO_2 composition retains the fluorite-related structure at room temperature and can be prepared free of m-ZrO_2 and the rhombohedrally distorted β-phase reported by Thornber *et al.* [10]. Compositions above ~ 8 mol % usually contain β-phase and compositions below about 7 mol % Sc_2O_3 contain m-ZrO_2 in addition to the fluorite-related phase [11].

0022–2461/83 $03.00 + .12

Considerable disagreement exists between various authors [6, 7, 12, 13] regarding the dependence of conductivity on temperature. A contribution from grain boundary impedance due to the presence of other phases and vacancy trapping by dopant cations, especially at low temperature, will undoubtedly influence the shape of the Arrhenius plots. In order to resolve these discrepancies several samples in the Sc_2O_3–ZrO_2 system with compositions close to 8 mol % Sc_2O_3 were prepared. Both 4-probe d.c. and complex impedance dispersion analysis techniques were used for the conductivity measurements. The results were supported by X-ray diffraction and dilatometry.

2. Experimental details

The materials used in the preparation of various samples were : ZrO_2 containing 2 wt % HfO_2 (Harshaw, > 99.5%, Loss on Ignition (LOI) = 0.84%), ZrO_2 (Koch Light > 99.8%, LOI = 0.79%), zirconium carbonate (Magnesium Elektron Limited – equivalent (ZrO_2 + 2 wt % HfO_2) > 99%). Sc_2O_3 (AMDEL Australia, 99.5%, LOI = 0.94%).

Most of the samples were prepared by thoroughly blending the oxide powders in the proper proportion. However, samples of 7.75 and 8 mol % Sc_2O_3–ZrO_2 were also made by coprecipitation of the hydroxides by ammonia from a solution containing scandium and zirconium nitrates, prepared by dissolving Sc_2O_3 and zirconium carbonate in nitric acid.

The coprecipitated or physically mixed oxide powders were normally calcined at 1100° C for 1 h. One batch of coprecipitated powder of 7.75 mol % Sc_2O_3–ZrO_2 was calcined at 800° C for 6 h. The calcined powders were compacted into bar shapes at a low pressure. These were then isostatically pressed at a pressure of 205 MN m^{-2} followed by sintering at 1700° C for 15 h in air in a tube furnace. Some sintered bars were given a further heat treatment at a higher temperature in a gas fired furnace. Except for sample A2 which was air quenched, all other samples were cooled slowly after higher temperature firings. Details of the preparation techniques and heat treatments are given in Table I.

The samples for 4-probe conductivity measurements were 20 to 30 mm long and had a diameter between 5 and 8 mm after cutting and grinding. The two end faces of the bars were ground flat, cleaned and painted with platinum paste (Hanovia Liquid Gold 6082 or Johnson Matthey Metal Ltd. N758). These were subsequently fired at 800° C to burn off the organic binder. Platinum foil contacts for passing current were attached to these paste electrodes later on. The probes for measuring the potential drop were constructed by cutting, with a diamond saw, a circular groove ~0.25 mm wide, ~0.2 mm deep and 5 to 7 mm away from each end, and wedging a 0.25 mm diameter platinum wire into each groove. In some cases the grooves were painted with platinum paste to ensure good electrical contact between the platinum wire and the ceramic body.

A constant current of 0.5 to 300 μA (depending upon the specimen resistance) was supplied by a Keithley constant current source model 227. All the current ranges were precalibrated and correction was applied during calculation of the conducductivity. For currents below 10 μA, the current through the specimen was determined by measur-

TABLE I Preparation details and results of m-ZrO_2 measurements

Specimen	Specimen starting composition§	Method of preparation	Heat treatment T(° C) (h)	% monoclinic† ZrO_2
A1	8 mol % Sc_2O_3 + 92 mol % ZrO_2	Coppt.	1700(34)	*
A2	8 mol % Sc_2O_3 + 92 mol % ZrO_2	Coppt.	1700(34), 2020(24)‡	*
B1	8 mol % Sc_2O_3 + 92 mol % ZrO_2	Mixed oxide	1700(15)	8
B2	8 mol % Sc_2O_3 + 92 mol % ZrO_2	Mixed oxide	1700(15), 2050(2), 1900(1)	*
C1	7.8 mol % Sc_2O_3 + 92.2 mol % ZrO_2	Mixed oxide	1700(15)	13
C2	7.8 mol % Sc_2O_3 + 92.2 mol % ZrO_2	Mixed oxide	1700(15), 1900(3)	*
C3	7.8 mol % Sc_2O_3 + 92.2 mol % ZrO_2	Mixed oxide	1700(15), 2050(2), 1900(1)	*
D1	7.75 mol % Sc_2O_3 + 92.25 mol % ZrO_2	Coppt.	2000(20)	*

*X-ray diffraction patterns of these samples do not show the presence of m-ZrO_2 lines.
†Errors in the estimation of m-ZrO_2 are typically ± 10% of the measured values.
‡Sample air quenched after last firing.
§Harshaw Zirconia was used in the preparation of samples, C1, C2 and C3 and Koch-Light Zirconia for samples B1 and B2.

ing the potential drop across a resistor of known value placed in series with the specimen. The potential drop across the potential probes was measured with a Keithley model 192 digital multimeter (input impedance 1000 MΩ). At lower temperatures when specimen resistance was high, a Keithley model 616 digital electrometer with input impedance $> 10^{14}\,\Omega$ was used. The total error due to probe positioning and instrumentation was less than 2%.

The specimens for 2-probe complex impedance measurements were 3 to 6 mm long and had a diameter between 5 and 8 mm. The construction of two electrodes for a.c. experiments was similar to that of the current probes in the 4 terminal d.c. conductivity samples. A Solartron frequency response analyser 1174 (frequency range 0.1 mHz to 1 MHz) interfaced to a Digital Equipment Corporation MINC 1123 minicomputer was used for complex impedance measurements. The voltage signal applied across the sample was usually below 20 mV rms.

4-probe d.c. conductivity measurements were made between 400 and 1000° C at 25° C temperature intervals over several heating and cooling cycles. The temperature range was between 350 and 800° C for a.c. measurements. After each temperature change sufficient time (45 to 60 min) was allowed for thermal equilibrium conditions to re-establish before recording data. In general, over the temperature ranges stated, the number of data points obtained for each heating or cooling cycle were 22 to 25 for 4-probe d.c. and 14 for complex impedance experiments.

All the measurements were performed in a flowing atmosphere of air or oxygen.

X-ray diffraction patterns of sintered discs from all the samples were taken with a Rigaku diffractometer using Cu$K\alpha$ radiation. To determine the total monoclinic content, the specimens were ground flat and polished before recording diffraction patterns. The integrated intensity method reported by Garvie and Nicholson [14] was used to measure m-ZrO_2. The areas under the monoclinic 1 1 1, 1 1 $\bar{1}$ and cubic 1 1 1 peaks were determined with a planimeter. No correction was applied for the Lorentz polarization factor. X-ray diffraction patterns of samples which were free of m-ZrO_2 were also taken with a Hagg–Guinier focusing camera using Cu$K\alpha_1$ radiation. Thoria was used as an internal standard for the purpose of determining accurate cell parameters [15].

Thermal expansion curves were recorded for some samples with a modified Gebruder Netzsche dilatometer at typical heating and cooling rates of 300° C h^{-1}. Slower cooling rates of 35 to 40° C h^{-1} made little difference to the results.

3. Results and interpretation

3.1. X-ray studies

X-ray diffraction patterns of the mixed oxide samples heated to 1700° C (15 h) showed the presence of m-ZrO_2 and a fluorite-related phase. Higher temperature firings of the sintered bars resulted in the disappearance of m-ZrO_2 lines for these samples. X-ray diffraction patterns of all the samples taken with the Hagg–Guinier camera showed slight tetragonal splitting of the fluorite lines. Phase equilibrium studies in the Sc_2O_3–ZrO_2 system for Sc_2O_3 concentrations between 4 and 9 mol% also indicated that the room temperature phase had the tetragonal symmetry [16]. In the present study coprecipitated samples of 7.75 and 8 mol% Sc_2O_3–ZrO_2 were indexed as tetragonal with no evidence of the presence of another phase. However, mixed oxide samples of 7.8 and 8 mol% Sc_2O_3–ZrO_2 showed minor concentrations of the β-phase as has been reported previously for comparable Sc_2O_3–ZrO_2 compositions [11]. The β-phase lines persisted even after extensive heat treatment and the presence of this phase is thought to be due to small compositional inhomogeneities in the samples. This view is supported by the observed complete disappearance of the β-phase in an 8.5 mol% Sc_2O_3–ZrO_2 sample after several successive firings to 1900° C, each firing being followed by crushing, grinding and repelletizing [17]. In addition to the presence of β-phase the mixed oxide samples showed less tetragonal distortion than the coprecipitated samples, an observation for which no explanation can be offered at this stage.

3.2. 4-probe d.c. conductivity and dilatometry results

Hysteresis effects and S-shaped Arrhenius conductivity curves were observed only for those samples (B1 and C1) which contained m-ZrO_2 at room temperature (Figs. 1 and 2). Dilatometry curves of these samples showed inflection(s) corresponding to the m-$ZrO_2 \rightleftharpoons$ t-ZrO_2 transformation. For samples which were free of m-ZrO_2, no hysteresis effects or S-shaped curves were observed in the Arrhenius plots (Figs. 1 to 3). Thermal expansion

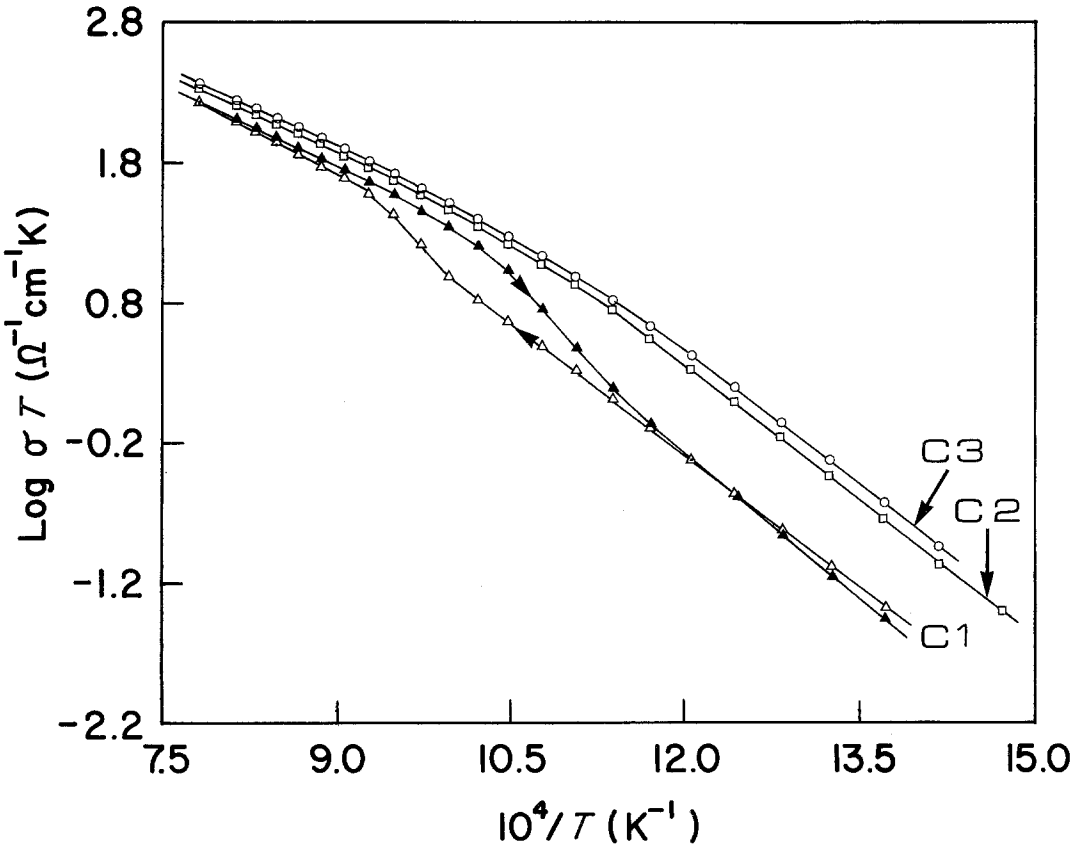

Figure 1 Arrhenius plots for samples C1, C2 and C3 of 7.8 mol % Sc_2O_3–ZrO_2 composition. Heating and cooling cycle data for samples C2 and C3 overlap.

curves of these samples also did not show any inflection and the conductivity data overlapped during successive heating and cooling cycles within experimental errors ($< \pm 2\%$). These observations clearly suggest that S-shaped curves and hysteresis effects in the Arrhenius plots of samples B1 and C1 are associated with the m-$ZrO_2 \rightleftharpoons$ t-ZrO_2 transformation.

The 4-probe d.c. conductivity data for six m-ZrO_2-free samples showed a distinct curvature in the Arrhenius plots (Figs. 1 to 3) towards a higher activation energy at lower temperatures (below ~600 to 625° C). The change in the slope was independent of the starting material, the method of preparation, heat treatments and of the presence (mixed oxides) or absence (coprecipitates) of minor amounts of the β-phase, indicating it to be an inherent property of the material.

The activation energies for all samples, calculated from a few data points at each end of the curve (for the high and the low temperature regions) using the Arrhenius relation $\sigma T = A \exp(-E/RT)$ are given in Table II. For samples which showed hysteresis effects, the activation energy for the high temperature regions was calculated using data from the cooling curve. The heating cycle data were used to calculate the activation energy for the low temperature region. The activation energy for the high temperature region was 71 to 75 kJ mol^{-1} whereas for the low temperature region it was 120 to 130 kJ mol^{-1} (see below).

3.3. Complex impedance dispersion analysis

Complex impedance measurements were made on three m-ZrO_2-free samples (A2, B2 and D1). In Fig. 4 are shown the complex impedance plane plots for all three samples at several temperatures. All samples produced a large arc due to grain impedance which was slightly distorted on the low frequency end of the electrolyte dispersion indicating a relatively small contribution from the grain boundary impedance. The details of the data analysis technique will be published elsewhere.

The typical Arrhenius plots for the total

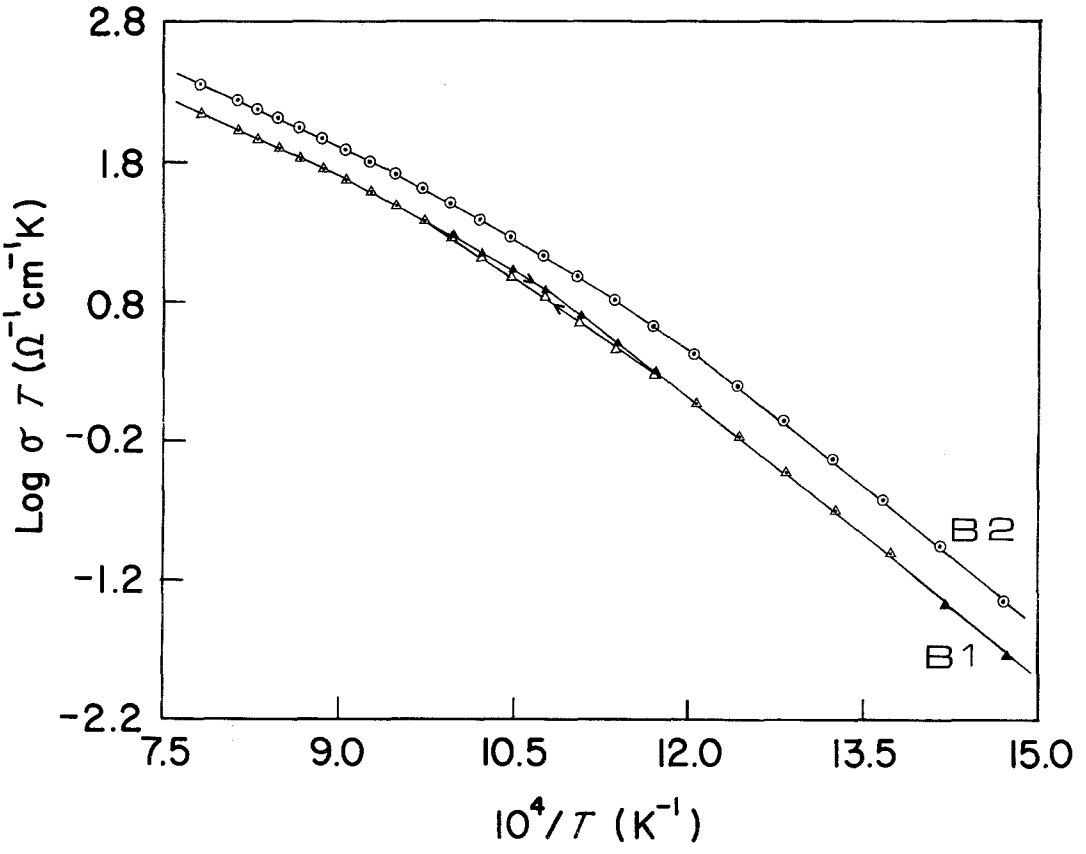

Figure 2 Arrhenius plots for samples B1 and B2 of 8 mol% Sc_2O_3–ZrO_2 composition. Heating and cooling cycle data for sample B2 overlap.

electrolyte conductivity and volume conductivity of the grains are plotted in Fig. 5. For the sake of clarity the data for only two samples have been plotted. The activation energies for the total electrolyte conductivity and volume conductivity of the grains in the low temperature region were quite similar and are given in Table III. This is not surprising considering the relatively small contribution from grain boundary impedance in these pure samples. The Arrhenius plots for the total electrolyte resistance showed a change in slope (Fig. 5) similar to that observed for the 4-probe d.c. conductivity data (Figs. 1 to 3). Moreover, activation energies for the total electrolyte resistance determined from both techniques agreed within experimental errors.

The relative unimportance of the grain boundary arc in samples free of m-ZrO_2 indicates quite clearly the absence of a low-conducting phase (phases) at the grain boundaries.

4. Discussion

Because of the complications arising due to the presence of m-ZrO_2 in samples B1 and C1, discussion of the results in this section will be restricted to those samples which were completely free of m-ZrO_2. The role of m-ZrO_2 will be discussed in a future publication.

Considering the small contributions from the grain boundary resistance in our m-ZrO_2-free samples it is reasonable to assume that the 4-probe d.c. technique measured the volume resistance of the grains. The 4-probe d.c. conductivity data for these samples could be best fitted to an equation of the form:

$$\rho = A_1 T \exp(E_1/RT) + A_2 T \exp(E_2/RT) \quad (1)$$

where ρ is the resistivity, A_1, A_2 are pre-exponential factors and E_1, E_2 are activation energies. Equation 1 recognizes contributions from two processes and has been used to describe either the effect of vacancy-dopant association or the contribution from grain boundary and volume resistance of the grains [18]. To demonstrate the accuracy with which Equation 1 fits the data, a comparison

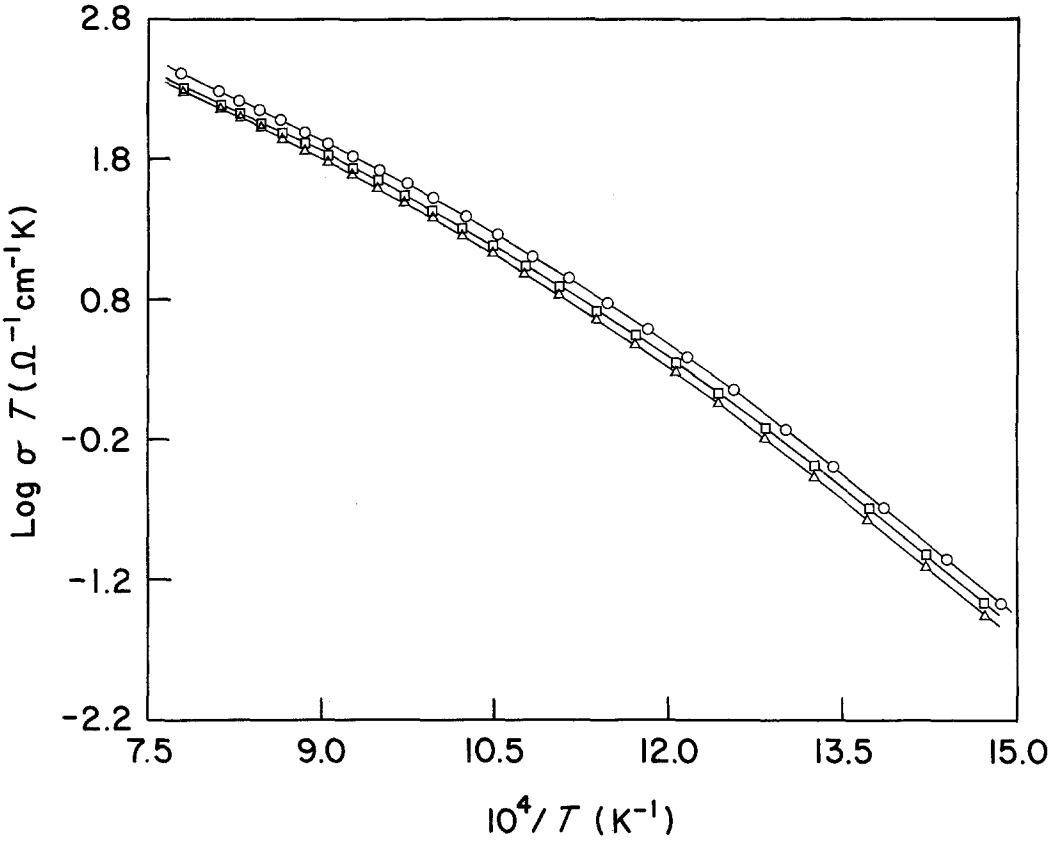

Figure 3 Arrhenius plots for coprecipitated samples: ○ – D1 of 7.75 mol% Sc_2O_3–ZrO_2 composition; □ – Al, △ – A2 of 8 mol% Sc_2O_3–ZrO_2 composition. Heating and cooling cycle data for all three samples overlap.

of experimental and calculated values of resistivities at several temperatures has been made in Table IV for two samples. Similar agreement between experimental and calculated data was obtained at other temperatures and for all other samples. The average error of fit was within the uncertainties of the experimental data. Values of E_1 and E_2 determined by fitting the data to Equation 1 and resistivities for all six samples are given in Table V. The values of activation energy reported in Table II for the high temperature region are slightly higher than E_1 and for the low temperature region are lower than E_2. This is probably due to the small contribution of one process in the temperature region chosen in Table II to calculate the activation energy for the second process. Thus the values of activation energy reported in Table V are the more accurate.

Changes in activation energy similar to those observed in the present work have been reported

TABLE II Activation energies of various samples for low and high temperature regions

Specimen	Activation energy*, (kJ mol^{-1})	
	High temperature region, 850–1000° C	Low temperature region, 400–550° C
A1	72 ± 2	123 ± 3
A2	75 ± 2	126 ± 3
B1	71 ± 2	126 ± 3
B2	72 ± 2	132 ± 3
C1	74 ± 2	121 ± 2
C2	73 ± 2	125 ± 2
C3	71 ± 2	124 ± 3
D1	75 ± 2	126 ± 3

*Calculated from $\sigma T = A \exp(-E/RT)$ relation.

TABLE III Activation energies from complex impedance data in the low temperature region (350 to 550° C)

Specimen	E^* (kJ mol^{-1}) for the total electrolyte resistance	E^* (kJ mol^{-1}) for the volume resistance of the grains
A2	123 ± 3	122 ± 3
B2	132 ± 3	134 ± 4
D1	132 ± 3	132 ± 3

*Determined from $\sigma T = A \exp(-E/RT)$ relation.

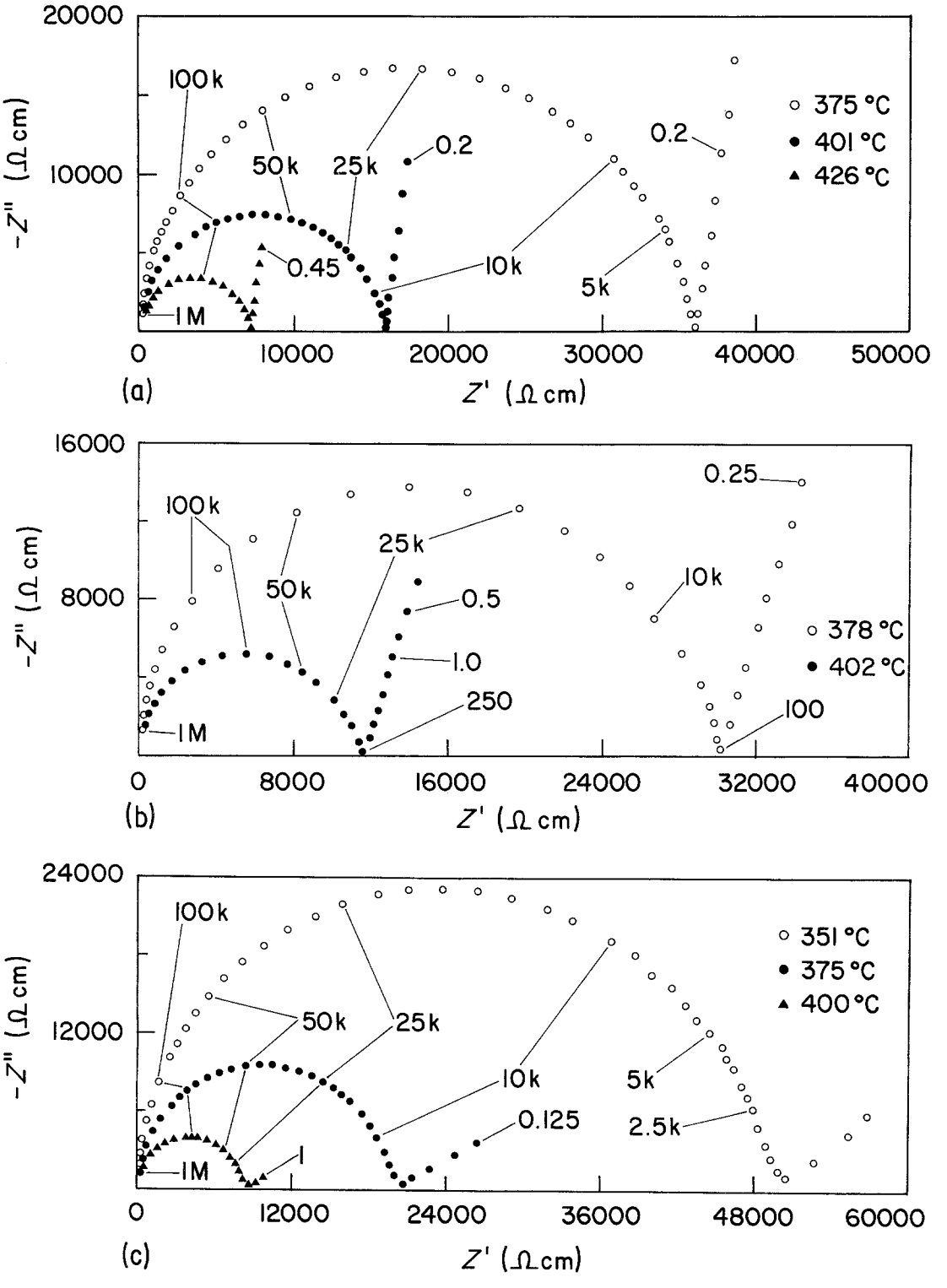

Figure 4 Complex impedance plots for (a) specimen A2, (b) specimen B2 and (c) specimen D1 at various temperatures in 100% oxygen. Numbers on the arcs are frequencies in Hz.

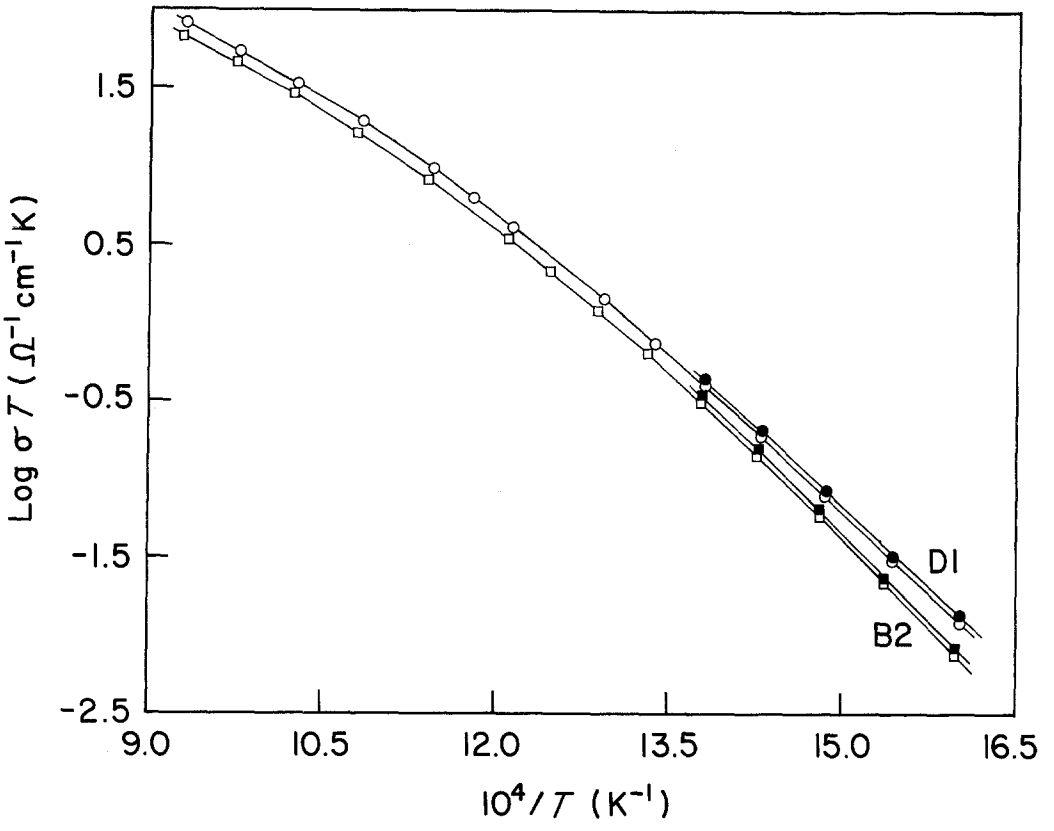

Figure 5 Arrhenius plots for the volume (closed symbols) and the total (open symbols) electrolyte resistance from complex impedance data for samples B2 and D1.

previously by several workers on zirconia or ceria-based systems although at different temperatures [19–21]. The results were interpreted as a changing dominance from grain boundary impedance at low temperatures to volume impedance of the grains at higher temperatures. In our samples contributions from grain boundary resistance were relatively small and therefore had little effect on the shape of the Arrhenius plots.

Alekseenko *et al.* [12] observed an inflection in the Arrhenius plot for 9 mol% Sc_2O_3–ZrO_2 corresponding to a change in the slope towards a higher activation energy below 630° C. From the high temperature X-ray work they concluded that this change in slope was due to the formation and disappearance of β-phase between 500 and 630° C. In order for the β-phase to have a significant influence on the shape of the Arrhenius plots it must be poorly conducting and present either at those locations (such as the interfaces between grains) from where it could exert maximum influence on the conductivity or it should be present in substantial proportion within the grains of the more conducting tetragonal phase. Our samples contained a relatively small amount of β-phase. Moreover, similar behaviour was observed for all six samples although X-ray studies indicated the presence of β-phase in only three samples, namely, B2, C2 and C3. Hence, the change in activation energy observed in the present work cannot be attributed to the influence of the β-phase.

On the other hand Gur *et al.* [6], after review-

TABLE IV Comparison of experimental and calculated (cf Equation 1) resistivities

Temperature (° C)	Specimen			
	B2		D1	
	$\rho_{exptl.}$ (Ω cm)	$\rho_{calc.}$ (Ω cm)	$\rho_{exptl.}$ (Ω cm)	$\rho_{calc.}$ (Ω cm)
400	20202	19505	15720	15619
500	1096	1104	911	924.5
600	159.8	158.5	140.9	139.7
700	44.5	44.5	39.9	40.2
800	18.71	18.74	16.98	16.85
900	9.88	9.90	8.74	8.77
1000	5.98	6.00	5.26	5.23

TABLE V Activation energies for two processes determined by fitting the 4-probe d.c. data to Equation 1, and resistivities at various temperatures

Specimen	ρ (Ω cm)*				Activation energy (kJ mol^{-1})		Density % of theoretical
	T (°C)				High temperature process	Low temperature process	
	100	800	600	450			
A1	6.6	20.6	180	4075	66 ± 2	132 ± 3	82
A2†	6.9	22.4	195	4720	68 ± 2	135 ± 3	90
B2	6.0	18.7	160	3920	66 ± 2	137 ± 3	79
C2	6.3	20.1	180	4670	64 ± 2	134 ± 3	85
C3	5.8	17.5	145	3570	65 ± 2	135 ± 3	87
D1	5.3	17.0	141	3370	70 ± 2	137 ± 3	94

*Resistivity values were not corrected for porosity.
†The slightly higher resistivity of this sample compared with A1 is mainly due to cracks which were produced by air quenching of sample A2.

ing the work of several authors, suggested that the contribution from grain boundary impedance is negligible in pure samples, and no change in slope should be observed in the Arrhenius curves. They concluded that such behaviour was an artifact of the measurement techniques used, i.e. a.c. measurements at a constant frequency of 1 kHz or d.c. measurements in which contributions from other polarization effects (e.g. electrode reactions, etc.) were not eliminated. They reported measurements on one sample of 8 mol % Sc_2O_3–ZrO_2 at only four temperatures between 600 and 900° C, fitting a straight line to their data on an Arrhenius plot. Their upper frequency limit was 20 kHz and it appears from their data that they observed mainly the electrode dispersion.

We agree with Gur *et al.* [16] that, in relatively pure Sc_2O_3–ZrO_2 free of low-conducting grain boundary phases, the contribution from grain boundary impedance is negligible and hence the left intercept of the electrode arc on the real axis approximates the true volume resistance of the grains. However, we carefully considered and separated the contributions of various polarization processes in the work reported here. Our 4-probe d.c. and complex impedance experiments were conducted on several well-characterized samples, over wide ranges of temperature and frequency, and these agree that there is a change in slope of the Arrhenius curves. Gur *et al*'s conclusion is contradicted; the change in slope is real and not an artifact of the measurement technique.

Because the change in slope is only apparent below 600° C, the 600 to 900° C temperature range used by Gur *et al.* was inadequate to draw any definite conclusions regarding the shape of Arrhenius plots, the conductivity processes or their activation energies. To illustrate, in Fig. 6 we plot our 4-probe d.c. data on several samples at only four temperatures between 600 and 900° C. They are readily fitted by the simple relationship $\sigma = A \exp(-E/RT)$ to give an apparent activation energy of 80 ± 4 kJ mol^{-1}, similar to the 90 kJ mol^{-1} reported by Gur *et al.* [6]. However, the true activation energy for the high temperature region is 64 to 70 kJ mol^{-1} (Table V) similar to that reported by Strickler and Carlson [8] for the range 800 to 1300° C.

We believe that the change in the slope of the Arrhenius plots near 600 to 625° C is due to a phenomenon intrinsic to the material with little contribution from grain boundary resistance. The likely explanation appears to be the vacancy trapping model proposed by Bauerle and Hrizo [18], Casselton [22] and Kilner and co-workers [23, 24]. In this model a significant proportion of vacancies are considered to be trapped by the dopant cation to form nonconducting complexes at lower temperatures. As the temperature increases more vacancies become free and mobile. Thus at higher temperatures when most of the defects are free, conductivity is determined mainly by the migration of oxygen ion vacancies. Verkerk *et al.* [25] observed a similar change in slope of the Arrhenius plots at 525° C for volume conductivity of Y_2O_3–ZrO_2 samples and attributed it to vacancy trapping.

5. Conclusions

S-Shape curves and hysteresis effects in the Arrhenius conductivity plots were observed in specimens containing m-ZrO_2 due to the m-$ZrO_2 \rightleftharpoons$ t-ZrO_2 transformation. The conducting phase was indexed as tetragonal at room temperature. Sam-

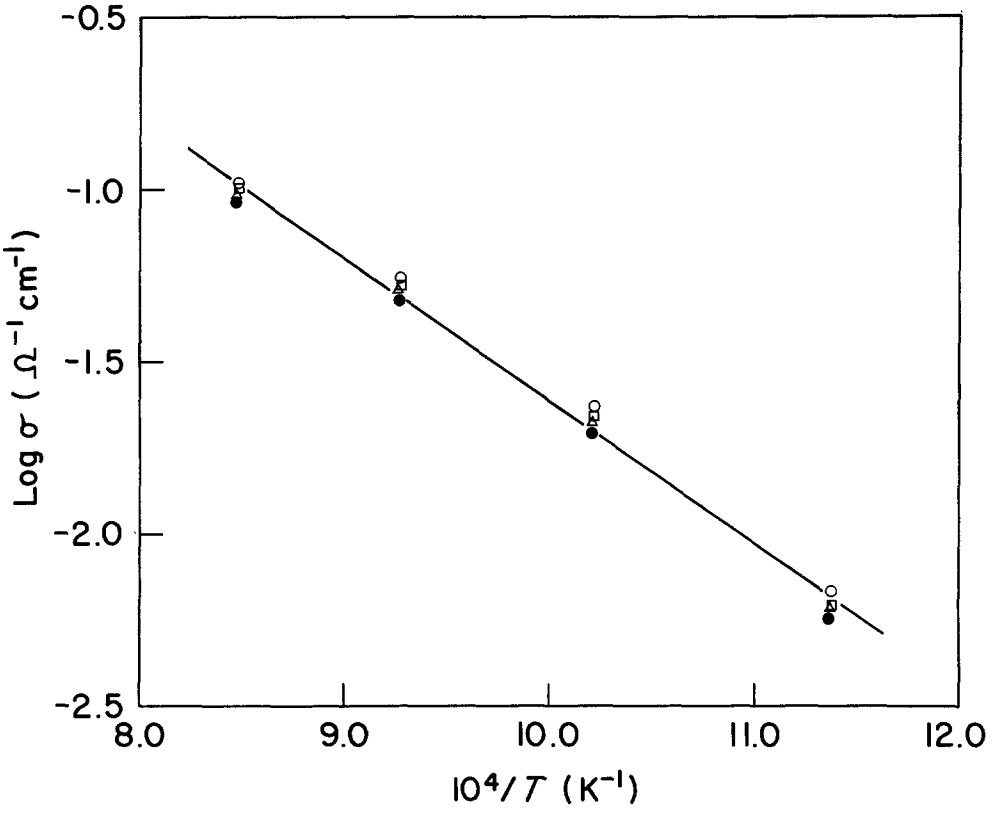

Figure 6 Arrhenius plot at four temperatures between 600 and 900° C for samples: ○ – B2, □ – C2, △ – Al, • – A2.

ples which were free of m-ZrO_2 showed a change in slope towards a lower activation energy at higher temperatures independent of the presence or absence of minor amounts of β-phase. This was attributed to the dissociation of vacancy traps as the temperature increased. The contribution from the grain boundary resistance in these pure samples was relatively small in comparison with the volume resistance of the grains. The activation energy for the migration of the oxygen ion vacancies was 64 to 70 kJ mol^{-1}.

Acknowledgements

The author wishes to acknowledge the assistance rendered by Mr F. T. Ciacchi, Mr R. K. Stringer and Miss B. Terrell in preparation of the samples. Many useful discussions with Dr M. J. Bannister and Mr W. G. Garrett are gratefully acknowledged. Drs M. J. Bannister, J. Drennen and Mr W. G. Garrett critically reviewed this manuscript. The author also wishes to express his gratitude to Assoc. Professor H. J. de Bruin for making software available for interfacing the Solartron frequency response analyser to a Minc 1123 minicomputer. Part of this work was supported by a grant from the National Energy Research Development and Demonstration Council of Australia.

References

1. H. OBAYASHI and T. KUDO, in "Solid State Chemistry of Energy Conversion and Storage", Advances in Chemistry Series, Vol. 163, edited by J. B. Goodenough and M. S. Whittingham (American Chemical Society, Washington, DC, 1977) p. 316.
2. W. DOENITZ and R. SCHMIDBERGER, *Int. J. Hydrogen Energy* 7 (1982) 321.
3. "Measurement of Oxygen, Proceedings of the Interdisciplinary Symposium", edited by H. Degn, I. Balslev and R. Brook (Elsevier, Amsterdam, 1976).
4. "Advances in Ceramics", Vol. 3, edited by A.H. Heuer and L. W. Hobbs (American Ceramic Society Inc., Columbus, Ohio, 1981).
5. J. E. BAUERLE, *J. Phys. Chem. Solids* **30** (1969) 2657.
6. T. M. GUR, I. D. RAISTRICK and R. A. HUGGINS, *Mater. Sci. Eng.* **46** (1980) 53.
7. F. M. SPIRIDONOV, L. N. POPOVA and R. Ya. POPIL'SKII, *J. Solid State Chem.* **2** (1970) 430.
8. D. W. STRICKER and W. G. CARLSON, *J. Amer. Ceram. Soc.* **48** (1965) 286.
9. J. LEFÈVRE, *Rev. Hautes Temp. Refrac.* **1** (1964) 229.

10. M. R. THORNBER, D. J. M. BEVAN and E. SUMMERVILLE, *J. Solid State Chem.* **1** (1970) 545.
11. E. SUMMERVILLE, PhD thesis, The Flinders University of South Australia (1973).
12. L. S. ALEKSEENKO, A. M. GAVRISH, N. V. GUL'KO, G. P. OREKHOVA, L. A. TARASOVA and N. K. POLNITSKAYA, *Russ. J. Inorg. Chem.* **26** (1981) 476.
13. Z. S. VOLCHENKOVA and V. M. NEDOPEKIN, *Izv Akad. Nauk SSSR Neorg. Mater.* **10** (1974) 1821.
14. R. C. GARVIE and P. S. NICHOLSON, *J. Amer. Ceram. Soc.* **55** (1972) 303.
15. H. G. SCOTT, *J. Mater. Sci.* **10** (1975) 1527.
16. M. J. BANNISTER and P. F. SKILTON, *J. Mater. Sci. Lett.* accepted.
17. P. F. SKILTON, CSIRO, Division of Materials Science, Internal Report No. AML-82-22.
18. J. E. BAUERLE and J. HRIZO, *J. Phys. Chem. Solids* **30** (1969) 565.
19. DA YU WANG and A. S. NOWICK, *J. Solid State Chem.* **35** (1980) 325.
20. S. H. CHU and M. A. SEITZ, *ibid.* **23** (1978) 297.
21. A. I. IOFFE, M. V. INOZEMTSEV, A. S. LIPILIN, M. V. PERFILEV and S. V. KARPACHOV, *Phys. Status Solidi A* **30** (1975) 87.
22. R. E. W. CASSELTON, *ibid.* **2** (1970) 571.
23. J. A. KILNER and R. J. BROOK, *Solid State Ionics* **6** (1982) 237.
24. J. A. KILNER and C. D. WATERS, *ibid.* **6** (1982) 253.
25. M. J. VERKERK, B. J. MIDDELHUIS and A. J. BURGGRAAF, *ibid.* **6** (1982) 159.

Received 21 January
and accepted 24 February 1983